3LP: a linear 3D-walking model including torso and swing dynamics

Salman Faraji[1] and Auke J. Ijspeert[1]

Abstract

In this paper, we present a new mechanical model for biped locomotion, composed of three linear pendulums (one per leg and one for the whole upper body) to describe stance, swing and torso dynamics. In addition to a double support phase, this model has different actuation possibilities in the swing hip and stance ankle which produce a broad range of walking gaits. Without the need of numerical time-integration, closed form solutions help to find periodic gaits which could simply scale in certain dimensions to modulate the motion online. Thanks to linearity properties, the proposed model can potentially provide a computationally fast platform for model predictive controllers to predict the future and consider meaningful inequality constraints to ensure feasibility of the motion. Such property is coming from describing dynamics with joint torques directly and therefore, reflecting hardware limitations more precisely, even in the very abstract template space. The proposed model produces human-like torque and ground reaction force profiles, and thus, compared to point-mass models, it is more promising for generation of dynamic walking trajectories. Despite being linear and lacking many features of human walking like CoM excursion, knee flexion, and ground clearance, we show that the proposed model can explain one of the main optimality trends in human walking, i.e. the nonlinear speed-frequency relationship. In this paper, we mainly focus on describing the model and its capabilities, comparing it with human data and calculating optimal human gait variables. Setting up control problems and advanced biomechanical analysis remains for future works.

Keywords

Bipedal Walking, Template model, Human-Like, 3D, Linear model

Introduction

Humanoid robots are challenging to control mainly due to their complex structures and a floating base. During locomotion tasks, these systems introduce another complexity compared to wheeled or flying robots, which is the hybrid nature of stepping where the continuous model changes in each phase. It has always been challenging to balance these robots with only unilateral supporting forces from the environment. Also, creating a sequence of motion, the associated timing and the required control architecture are other important topics in controlling humanoid robots. The main objectives are therefore being human-like, energy efficient, versatile and of course agile like humans. In this paper, we are proposing a new template model that describes main aspects of walking while being computationally very efficient. Such model can be very useful in modern control architectures from the computational perspective. It can also go beyond conventional template models such as Linear Inverted Pendulum (LIP) by producing more natural motions and faster walking speeds, resembling human locomotion.

The design of controllers should address many concerns like fast implementation, stability, robustness to unknown model parameters and the degree of dependency on sensory data. Besides, it is desired to handle speed transitions and large disturbance rejection in the same control framework. Candidate methods are typically coming with proper identification of the basin of attraction regarding system states, actuator limitations and violation of model assumptions. This identification is not always straightforward due to its nonlinear nature, though it has been postulated that two steps are enough to stabilize in almost all conditions (Zaytsev et al. 2015). In this regard, Model Predictive Control (MPC) is a powerful framework as it can find optimal policies constrained to certain actuation and state limitations. It can also predict if there is no feasible solution, to let the algorithm take a different decision.

Hierarchical controllers

Recently, hierarchical control approaches are becoming popular, where a simple template model determines the overall dynamics in an abstract way and then, a detailed full-body inverse dynamics controller converts this behavior to individual actuator inputs (Faraji et al. 2014; Feng et al. 2013; Kuindersma et al. 2014). In dynamical systems, prediction of future evolution is mainly sensitive to the model and sensory data precision (Bhounsule et al. 2015). In hierarchical approaches similarly, dynamical matching between the template and the full model is crucial to ensure precise execution of the abstract plan. In this regard, we briefly review relevant template models proposed for walking, identify missing properties and motivate the new model proposed in this paper.

[1]EPFL, Switzerland

Corresponding author:

Salman Faraji, EPFL STI IBI-STI BIOROB, Station 9, CH-1015 Lausanne, Switzerland

Email: salman.faraji@epfl.ch

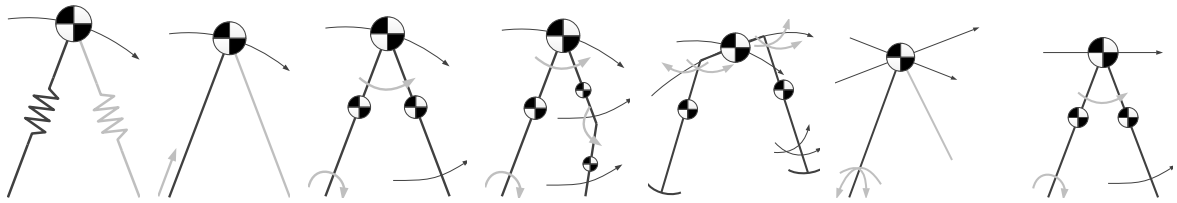

	(Iida et al. 2009)	(Hemami and Golliday 1977)	(Asano et al. 2004)	(Asano et al. 2004)	(Kuo 1999)	(Kajita and Tani 1991)	(Takenaka et al. 2009)
name	SLIP	IP	-	-	-	LIP	-
knee	-	-	-	x	-	-	-
steering	-	-	-	-	-	x	-
3D	-	-	-	-	x	x	-
smooth	x	-	-	-	-	x	x
torso	-	-	-	-	-	-	-
swing	-	-	x	x	x	-	x
linear	-	-	-	-	-	x	-

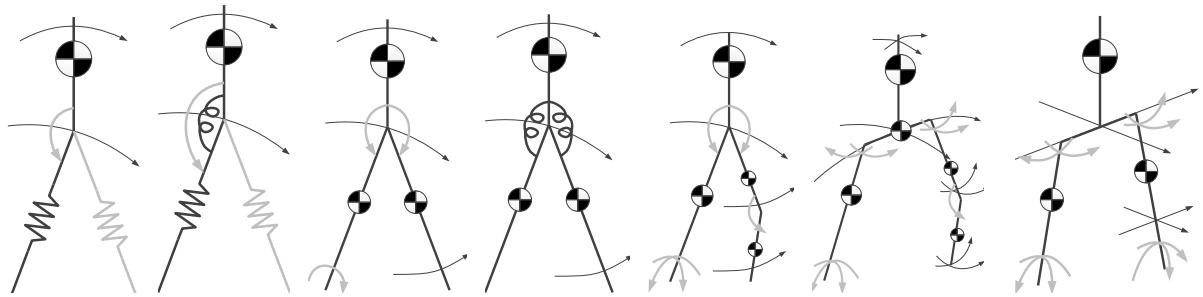

	(Maufroy et al. 2011)	(Sharbafi and Seyfarth 2015)	(Hasaneini et al. 2013)	(Gomes and Ruina 2011)	(Manchester and Umenberger 2014)	(Gregg et al. 2012)	proposed
name	BSLIP	FMCH	-	-	-	-	3LP
knee	-	-	-	-	x	x	-
steering	-	-	-	-	-	x	(x)
3D	-	-	-	-	-	x	x
smooth	x	x	-	x	-	-	x
torso	rotating	rotating	rotating	rotating	rotating	rotating	fixed
swing	-	-	x	x	x	x	x
linear	-	-	-	-	-	-	x

Figure 1. Different key models introduced in the literature for walking. In this table, the model is standing on the left leg, and the right leg is in the swing motion. Solid arrows show the direction of motion and degrees of freedom while gray arrows show actuation torques or push-off forces. For models without swing dynamics, we show the swing leg in gray color to implicitly indicate that attack angle is a control authority. Note that some of these models are only in 2D while more advanced models are in 3D. Some models simulate pelvis width, torso dynamics or ground clearance as well. Most of these models produce compass gait. However, some have ankle actuation or arc foot. In the comparison table, we mention important features such as knee flexion (for ground clearance), steering capabilities, 3D formulations, smooth profiles, the inclusion of torso and swing dynamics and linearity. By smoothness, we mean no collision and push-off impulse, but possibly describing the double support phase. Many of these models allow for torso pitch while we keep it fixed in 3LP for simplicity. Note that 3LP can describe steering like our previous work with LIP (Faraji et al. 2014), only if pelvis width is set to zero. Despite being linear, 3LP offers many features not existing in other template models.

Inverted Pendulums

One of the earliest template models that roughly explains bipedal mechanics is Inverted Pendulum (IP) (McGeer 1990). In this model, a single mass rolls over a massless stick with a fixed length. IP is widely used to analyze passive walkers (McGeer 1990) and energetics of human walking (Kuo et al. 2005). Inspired by IP, many simple robots are built to walk naturally with minimal energy, injected in push-off, swing hip or both (Collins et al. 2005). Later, this model was simplified to Linear Inverted Pendulum (LIP) (Kajita et al. 2003), favoring analytical solutions instead of numerical integrations. With a proper modulation of Zero Moment Point (ZMP) (Sardain and Bessonnet 2004), many position controlled robots like ASIMO (Sakagami et al. 2002)

perform walking via inverse kinematics methods. These algorithms are usually able to produce slow to moderate walking speeds. However, robots using the LIP method usually walk with crouched knees to keep the Center of Mass (CoM) at a constant height. In addition to increasing energy consumption, it is harmful to the robot in the long term and less human-like, though providing full controllability.

More recent extensions of LIP contain one (Park and Kim 1998) or two additional masses (Takenaka et al. 2009; Buschmann et al. 2007) in the legs to address swing dynamics while keeping the CoM height constant. For instance, in these extensions, the proposed model is formulated in a 2D space, and parameterized swing trajectories (in the sagittal and vertical planes) are used to generate desired gaits. In (Park and Kim 1998) specifically, sinusoidal profiles lead to closed form solutions with few realistic approximations introduced. Despite the advantage of describing ground clearance effects with a minimal coupling to the sagittal dynamics, the swing trajectory is yet imposed to the system, which is not desirable. We look for a more generic model to work at different speeds and frequencies, not relying on parametric trajectories to tune.

Multi-link pendulums

Apart from these single-mass models, there are other nonlinear extensions solved numerically. In (Byl and Tedrake 2008; Asano et al. 2004), the IP model was extended to have two separate masses for each leg as well as a single mass at the hip level. Using similar actuation schemes, this model could produce compass gaits on 2D-constrained robots. In (Asano et al. 2004), the same model was modified to have another Degree of Freedom (DoF) in the swing leg to provide ground clearance. The stance leg, however, always remains straight in this version. In (Westervelt et al. 2007), this model was augmented with a torso and later, it was also used by (Manchester and Umenberger 2014) to perform natural walking on uneven terrain, using a library of motion primitives. Another model with four masses in the legs, hip, and torso was proposed in (Gregg and Spong 2009) without any DoF in the stance knee. This model was used to generate walking trajectories with steering properties.

Aiming at removing impacts, a simpler model with two passive springs in the hips was proposed by Gomes (Gomes and Ruina 2011). These springs are mainly motivated by elastic properties of human muscles. By exploiting torso motions, Gomes could find zero energy gaits. Another interesting complex model was proposed in (Gregg et al. 2012) with a pelvis of a certain width in 3D and a mass in the center. The swing leg also had a DoF in the knee. This 3D model takes advantage of a limited transversal wrench in the contact point to facilitate steering. However, finding a periodic gait for such complicated model is difficult and computationally expensive.

Spring-Loaded Pendulums

It is always questionable which template model produces more realistic motion from the viewpoint of geometry, torques or energy. The models above mainly address energetic and geometric similarities. However, specific ground reaction force profiles and the elastic behavior observed in human legs are better produced in another category of models based on Spring Loaded Inverted Pendulum (SLIP) (Blickhan 1989). The simplest model in this category is composed of two massless springs (legs) connected to a point mass. Observations indicate a better description of energy exchange in this model over faster walking speeds and running, mimicking compliant properties of human tendons (Blickhan 1989). Based on this model, Iida (Iida et al. 2009) built a hip-actuated robot walking in 2D with various springs, similar to the human muscles. Properties of the passive SLIP itself -without hip actuation- were widely explored later in (Rummel et al. 2010). Using the concept of Virtual Pivot Point (VPP) to stabilize the torso, the model was also extended to have an upper body (Sharbafi and Seyfarth 2015) which made the motion more human-like.

In Figure.1, we have briefly shown key models proposed for walking in the literature. Note that in some of them, passive springs are added to the hip actuators for energy storage, similar to human. In this paper, however, we do not investigate elastic behaviors and energy-saving mechanisms.

Control difficulty

Except for LIP, all other models presented earlier require numerical integration to obtain time trajectories. Therefore, in a periodic walking paradigm, the Jacobian around a nominal solution linearizes the model and provides the framework for Floquet analysis or discrete controller designs (Rummel et al. 2010). This approach can be used to create an optimal library of primitives (Kelly and Ruina 2015; Manchester and Umenberger 2014; Gregg et al. 2012). However, online reaction to disturbances as well as the inclusion of other inequality constraints that are often ignored in calculating a stable basin of attraction limit the generality of this framework. MPC, on the other hand, is powerful in this regard. However, it requires simple and possibly linear models to facilitate online calculations. The LIP model, therefore, fits best in the MPC framework (Faraji et al. 2014; Herdt et al. 2010). MPC, its simpler version LQR, and sometimes Discretized LQR (DLQR) (Ogata 1995) controllers are popular in stabilizing walking gaits and recovering large pushes (Kelly and Ruina 2015; Byl and Tedrake 2008). With nonlinear models, however, a library of optimal policies is generated offline, or a discrete transition model is considered at specific events like CoM apex or heel-strike. Such controllers can not react to perturbations very quickly, since adjusting the plan is not computationally affordable online.

Why 3LP?

In this paper, we propose a more general version of LIP (Kajita et al. 2003) with three linear pendulums (called 3LP) that capture torso and swing dynamics in 3D. This model allows prediction of future at any time in closed form which is favorable by limited computational resources and MPC. Compared to LIP, 3LP-based trajectories are easier to track by inverse dynamics block in a hierarchical controller. In other words, CoM motion becomes more natural for the humanoid robot, since swing and torso dynamics are taken into account. Swing-leg trajectories are also more natural

compared to the template models which track an imposed angle of attack with a stiff controller (Kelly and Ruina 2015; Byl and Tedrake 2008; Collins et al. 2005). Besides, using 3LP, one can define meaningful torque limits in MPC frameworks instead of putting vague timing or step-size limits which do not precisely reflect physical facts about the real hardware. It should be noted, however, that the CoM height in 3LP is constant similar to LIP.

The 3LP model provides direct access to the hip and ankle torques. These input dimensions let us find various types of gaits with simple closed form expressions. 3LP as a template model is therefore very useful for motion planning. Along with falling dynamics like IP (Kuo et al. 2005) and LIP (Kajita et al. 2001), torso-balancing hip torques are also part of 3LP like (Maufroy et al. 2011). The most outstanding feature of 3LP is in considering swing dynamics in a linear fashion that allow us to calculate natural cycles. With LIP, however, a reference footstep plan is needed (Faraji et al. 2014). Considering Figure.1 again, few models in the literature consider this integral part of walking. In these models, due to nonlinearity, numerical integration is always needed to search for periodic gaits. In 3LP, however, we do not need to integrate the system or to perform numerical optimizations.

This paper merely focuses on introducing the model, formulating equations, finding gaits and comparing them to human gaits. Setting up control problems remain for future works. In the next section, we will explain model details and the assumptions behind. Next, a method based on geometrical symmetry is introduced to find different periodic gaits. We will demonstrate that for a human-like gait, actuation profiles in 3LP are similar to those in human. Finally, we show that 3LP, despite being linear, quantitatively explains the main optimality trend in human gaits, i.e. speed-frequency relation.

3LP dynamics

To capture the coupling of swing and torso dynamics, we have added two other pendulums to the standard LIP model, connected with a pelvis of a certain width. In this model, as shown in Figure.2, there are 2-DoF actuators in each hip and ankle. We visualize feet of limited size in Figure.2, only to mention the availability of ankle torques. The upper body (referred to as torso) and the legs are each represented by a single mass. By construction (assuming ideal controllers), masses stay in horizontal planes of constant height and the torso is always upright without sagittal, frontal or transversal rotations. These assumptions are used in (Gregg et al. 2012) as well to decouple sagittal and lateral dynamics.

Since the torso is connected to an accelerated frame (i.e. pelvis), a balancing torque is always needed to keep the torso upright. This torque is often calculated using the virtual pendulum concept (Sharbafi and Seyfarth 2015), where the torso can pitch or roll freely. Inspired by rolling contact constraints that produce more human-like gaits (Hamner et al. 2013), we allow for a transversal wrench at stance foot to help to keep the pelvis orientation fixed. In 3LP, we do not consider steering properties as they make the model nonlinear. It is practically easy however to steer the robot using an inverse dynamics layer, as we showed in (Faraji et al. 2014) where a simple LIP model was used. There is no need to add heel-strike and push-off impulses in 3LP since our double support phase smoothly takes care of the contact transition. In SLIP-based models (Sharbafi and Seyfarth 2015), the compliant springs automatically produce a double support phase and perform weight transition without impulses. In 3LP, however, switching to double support is triggered when both horizontal components of the swing foot velocity become zero. This assumption is typically used in models with swing dynamics like (Gomes and Ruina 2011), though unlike 3LP, Gomes removes double support for more simplicity (Gomes and Ruina 2011).

In Figure.2, all external/internal forces and torques, as well as positions, are shown for each interesting point of the model, i.e. contacts, hips and pelvis center. These vector variables in our model are expressed in the Cartesian frame. One can easily write geometric relations as:

$$\begin{aligned}
x_1 &= [x_{1,x} \;\; x_{1,y} \;\; 0]^T + h_1 \, \hat{z} \\
x_2 &= x_1 + (\frac{w_p d}{2}) \, \hat{y} \\
x_3 &= x_1 - (\frac{w_p d}{2}) \, \hat{y} \\
X_1 &= x_1 + h_4 \, \hat{z} \\
X_2 &= [X_{2,x} \;\; X_{2,y} \;\; 0]^T \\
X_3 &= [X_{3,x} \;\; X_{3,y} \;\; 0]^T \\
y_1 &= x_1 + h_3 \, \hat{z} \\
y_2 &= x_2 + \frac{h_2}{h_1}(X_2 - x_2) \\
y_3 &= x_3 + \frac{h_2}{h_1}(X_3 - x_3)
\end{aligned} \tag{1}$$

where w_p denotes pelvis width, phase variable $d = \pm 1$ depends on left or right support phases, $\hat{y} = \begin{bmatrix} 0 & 1 & 0 \end{bmatrix}^T$ points left, $\hat{z} = \begin{bmatrix} 0 & 0 & 1 \end{bmatrix}^T$ points up, h_1 is pelvis height, h_2 is relative leg mass height, h_3 is relative torso mass height and offset variable h_4 from the pelvis indicates the point where an external perturbation is applied. These parameters as well as other position variables are shown in Figure.2. We can write total force equations for each mass $i = 1, 2, 3$:

$$m_i(\ddot{y}_i + g) = f_i + F_i \tag{2}$$

where g denotes gravity and $m_2 = m_3$, assuming a symmetric model. The vectors F_i and f_i represent external and internal forces respectively. The total moment equations for each mass $i = 1, 2, 3$ are:

$$(X_i - y_i) \times F_i + (x_i - y_i) \times f_i + T_i + \tau_i = 0 \tag{3}$$

where vectors T_i represent external wrenches and τ_i represent internal torques, all defined in the Cartesian frame (refer to Figure.2). Finally, we can write total force and moment equations for the mass-less pelvis around the center point:

$$\begin{aligned}
f_1 + f_2 + f_3 &= 0 \\
\tau_1 + \tau_2 + \tau_3 + (x_2 - x_1) \times f_2 + (x_3 - x_1) \times f_3 &= 0
\end{aligned} \tag{4}$$

which link all variables together. In these equations, we consider X_1, X_2, X_3 as independent variables and solve for

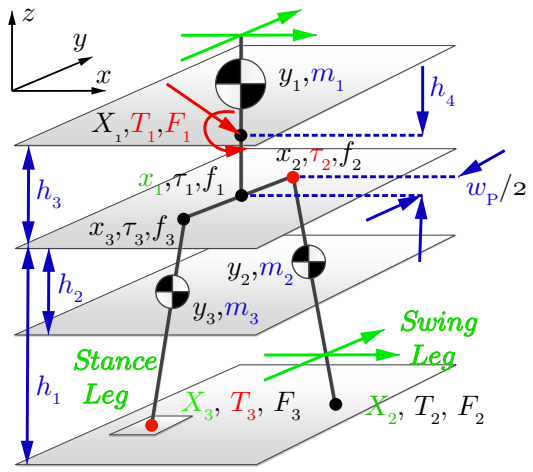

Figure 2. A schematic of 3LP model with all variables and model parameters. The bottom plane shows level ground and all upper planes of fixed height show where the three masses and the pelvis are constrained to move. The torso is always upright, and the pelvis is along the y-axis by model construction. The swing foot remains inside the bottom plane, i.e. sliding on the ground with no force during the swing phase. Note that in single support all contact forces for the swing leg (T_2, F_2) are zero. The inputs of the model are τ_2 and T_3 shown in red together with arbitrary external perturbations T_1 and F_1 applied to the torso. State variables are feet and pelvis positions, shown in green. Fixed model parameters are also shown in blue, including masses and geometrical dimensions.

others as dependent variables. Actuation possibilities for 3LP are selected as stance foot T_3 and swing hip torques τ_2 in the sagittal and lateral planes. Note that T_1 and F_1 represent disturbing external forces (at point X_1 on the torso) which are zero in normal conditions.

Now, differential equations governing the bipedal motion could be obtained for different phases. We consider a full stride, consisting of a double support followed by a single support phase, defined in Table.1. In double support, the weight is transferred from F_2 to F_3, and in single support, the leg with variables of subscripts 2 will swing forward. Over the next full stride phase, the supporting leg can be simply changed by altering the sign of variable d.

Full stride =	double support +	single support
duration	t_{ds}	t_{ss}
timing order	1	2
stance leg	subscripts 3	subscripts 3
swing leg	-	subscripts 2
control input	ankle	hip/ankle
controllability	over-actuated	fully-actuated

Table 1. Sequencing information about the two consecutive phases that form a full stride phase.

The equations (2), (3) and (4) are not enough to solve the system completely. We require 12 new equations to find all accelerations in terms of control inputs and vice versa. This number comes from the fact that in total, we have 12 actuation variables in the system (torques in the hips and ankles). In single support, since the system is fully actuated, the additional constraints can simply be added by considering zero contact force in the swing foot and zero acceleration in the stance foot. In double support, however, because of the inherent redundancy, we need to make assumptions to simplify the system.

Single support

In this phase, the swing foot does not have any external forces and the stance foot is fixed on the ground:

$$F_2 = 0,\ T_2 = 0,\ \ddot{X}_3 = 0 \tag{5}$$

To further simplify the system, we consider two modes of input torques: constant (U) and ramp (V) profiles. Despite being linear, these profiles can still lead to a convincing match with human torque profiles, discussed in the next section. More complex terms might improve the matching precision, but make the equations more complicated. Besides, since there are fundamental geometric differences between the limbs in 3LP and human (e.g. the number of articulated joints), higher order terms might lead to an over-fitting which is not desired. Overall, we have eight input parameters U and V in the system:

$$\begin{bmatrix}\tau_{2,y}\\ \tau_{2,x}\\ T_{3,y}\\ T_{3,x}\end{bmatrix} = \begin{bmatrix}U_{h,y}\\ U_{h,x}\\ U_{a,y}\\ U_{a,x}\end{bmatrix} + \frac{t}{t_{ss}}\begin{bmatrix}V_{h,y}\\ V_{h,x}\\ V_{a,y}\\ V_{a,x}\end{bmatrix} = U + \frac{t}{t_{ss}}V \tag{6}$$

where t_{ss} stands for single support duration, t denotes the time from the beginning of the single support phase, and subscripts a and h denote ankle and hip respectively. Equations of (5) and (6) together give 12 additional constraints that enable us to solve the system completely. To this end, we define the state vector $X^{ss}(t)$ and the disturbance vector W as:

$$\begin{gathered}X^{ss}(t) = \\ \begin{bmatrix}X_{2,x}(t) & X_{2,y}(t) & x_{1,x}(t) & x_{1,y}(t) & X_{3,x} & X_{3,y}\end{bmatrix}^T \\ W = \begin{bmatrix}F_{1,x} & F_{1,y} & T_{1,y} & T_{1,x}\end{bmatrix}^T\end{gathered} \tag{7}$$

where X_3 is the fixed contact point location. Using Maple (Monagan et al. 2005), we combine all equations and obtain a linear DAE system symbolically:

$$\begin{aligned}\frac{d^2}{dt^2}X^{ss}(t) \;=\; & C^{ss}_X\, X^{ss}(t) + \\ & C^{ss}_U\, U + C^{ss}_V\, V + C^{ss}_W\, W + C^{ss}_d\, d\end{aligned} \tag{8}$$

where constant matrices C^{ss} merely depend on system parameters (refer to Appendix A for further details). In this equation, $X^{ss}(t)$ is the state vector, U and V represent constant and ramp inputs, W represents perturbations and d denotes the phase variable. Next, we define the full state vector $Q^{ss}(t)$ and the constant vector R as:

$$\begin{aligned}Q^{ss}(t) &= \begin{bmatrix}X^{ss}(t)^T & \dot{X}^{ss}(t)^T\end{bmatrix}^T \\ R &= \begin{bmatrix}U^T & V^T & W^T & d\end{bmatrix}^T\end{aligned} \tag{9}$$

Such abstract formulation facilitates the process of finding periodic gaits, discussed in the next section. Assuming constant external forces W, we can solve this system

analytically:

$$Q^{ss}(t) = A^{ss}(t)\, Q^{ss}(0) + B^{ss}(t)\, R \tag{10}$$

where the time-dependent transition matrices $A^{ss}(t)$ and $B^{ss}(t)$ describe state evolution over time. These matrices are in fact very easy to calculate, because of their simple structure:

$$\begin{aligned} A^{ss}(t) &= \sum_{i=1}^{6} A_i^{ss} \gamma_i^{ss}(t) \\ B^{ss}(t) &= \sum_{i=1}^{6} B_i^{ss} \gamma_i^{ss}(t) \end{aligned} \tag{11}$$

where $\gamma_i^{ss}(t) = e^{w_i^{ss} t}$ for $i = 1..4$, $\gamma_5^{ss}(t) = 1$ and $\gamma_6^{ss}(t) = t$. The four scalars w_i^{ss} are square roots of the eigenvalues associated to the non-zero part of C_X^{ss} matrix (which has 4 dimensions). These values describe falling and swing dynamics, quantifying instability and divergence properties. A shorter pelvis height, for example, leads to w_i^{ss} values with larger magnitudes which mean that falling and swing dynamics become faster. A_i^{ss} and B_i^{ss} merely depend on constant system parameters, encoding evolution of the initial state and the effect of inputs respectively. Once these individual matrices are calculated offline, $A^{ss}(t)$ and $B^{ss}(t)$ can be easily calculated online by few arithmetic operations. Note that in 3LP, lateral and sagittal dynamics are decoupled, but their similarity leads to repeated eigenvalues.

Double support

In this phase, the two feet are fixed:

$$\ddot{X}_3 = 0,\ \ddot{X}_2 = 0 \tag{12}$$

and contact forces are being transfered from (F_2, M_2) to (F_3, M_3). Once (F_2 and M_2) become zero, the next single support phase starts, where the leg with subscript 2 performs swing motion. So far, equations (12) give us only 4 constraints, while 8 are yet missing.

In double support, we decided a linear transfer of weight from one leg to another. This means the vertical component of the Ground Reaction Force (GRF) in the previous stance leg (which has been stationary during single support) will go linearly to zero during double support. Such straightforward policy provides simple analytic solutions (compared to quadratic or other forms). Assume that:

$$\begin{bmatrix} F_{2,z} \\ T_{2,z} \end{bmatrix} = (1 - \frac{t}{t_{ds}}) \begin{bmatrix} \alpha(t) \\ \beta(t) \end{bmatrix}, \begin{bmatrix} F_{3,z} \\ T_{3,z} \end{bmatrix} = \frac{t}{t_{ds}} \begin{bmatrix} \alpha(t) \\ \beta(t) \end{bmatrix} \tag{13}$$

where t_{ds} denotes double support duration and t denote the time from the beginning of the double support phase. The variables $\alpha(t)$ and $\beta(t)$ are (possibly complex) functions of other variables in the system, but we are not going to find them explicitly. The linear policy can be encoded with the following equations by removing $\alpha(t)$ and $\beta(t)$:

$$\frac{t}{t_{ds}} \begin{bmatrix} F_{2,z} \\ T_{2,z} \end{bmatrix} = (1 - \frac{t}{t_{ds}}) \begin{bmatrix} F_{3,z} \\ T_{3,z} \end{bmatrix} \tag{14}$$

Remember that in single support, the ankle torques in the stance foot are determined by (6) and the vertical GRF is constant (because of the fixed height assumptions in the model). Given that the vertical GRF decreases linearly with time, the Center of Pressure (CoP) position can be simply preserved in double support by linearly decreasing contact reaction moment T_2 in stance leg (and increasing T_3 accordingly):

$$\begin{aligned} \begin{bmatrix} T_{2,y} \\ T_{2,x} \end{bmatrix} &= (1 - \frac{t}{t_{ds}}) \begin{bmatrix} U_{a,y} + V_{a,y} \\ -U_{a,x} - V_{a,x} \end{bmatrix} \\ \begin{bmatrix} T_{3,y} \\ T_{3,x} \end{bmatrix} &= \frac{t}{t_{ds}} \begin{bmatrix} U_{a,y} \\ -U_{a,x} \end{bmatrix} \end{aligned} \tag{15}$$

The equations (15) together with (6) will indeed result in piecewise linear ankle torque profiles. Note that the minus signs behind the lateral-plane ankle torques $U_{a,x}$ and $V_{a,x}$ in (15) come from the symmetry concept in the lateral plane. In other words, we assume that these constants move the CoP in opposite directions in the two feet. A positive $U_{a,x}$ for example moves the CoP to the left on the left foot, while moving it to the right on the right foot.

Similarly to (13), we implement a transition policy for the hip torques as well. Assume that:

$$\begin{aligned} \tau_{2,y} &= (\frac{t}{t_{ds}}) U_{h,y} + (1 - \frac{t}{t_{ds}}) \gamma(t) \\ \tau_{3,y} &= (1 - \frac{t}{t_{ds}})(U_{h,y} + V_{h,y}) + (\frac{t}{t_{ds}}) \gamma(t) \end{aligned} \tag{16}$$

where $\tau_{2,y}$ starts from a function $\gamma(t)|_{t=0}$ in the beginning and converges to $U_{h,y}$ at the end of double support phase. Likewise, $\tau_{3,y}$ starts from $(U_{h,y} + V_{h,y})$ and converges to the same $\gamma(t)|_{t=t_{ds}}$ at the end of the phase. The function $\gamma(t)$ in fact represents the torque in the stance hip which is a complex function of other variables in the system. However, we know linear trajectories of swing hip torques from (6). The equation (16) therefore encodes a linear transition policy. Similar rules can be written for the lateral plane.

$$\begin{aligned} \tau_{2,x} &= (\frac{t}{t_{ds}}) U_{h,x} + (1 - \frac{t}{t_{ds}}) \zeta(t) \\ -\tau_{3,x} &= (1 - \frac{t}{t_{ds}})(U_{h,x} + V_{h,x}) + (\frac{t}{t_{ds}}) \zeta(t) \end{aligned} \tag{17}$$

where the minus sign (behind $\tau_{3,x}$) is for symmetry, like before. The function $\zeta(t)$ plays the same role as $\gamma(t)$, but in the lateral plane. Now, we can remove $\gamma(t)$ and $\zeta(t)$ to make more explicit equations:

$$\begin{aligned} \frac{\tau_{2,y} - \frac{t}{t_{ds}} U_{h,y}}{1 - \frac{t}{t_{ds}}} &= \frac{\tau_{3,y} - (1 - \frac{t}{t_{ds}})(U_{h,y} + V_{h,y})}{\frac{t}{t_{ds}}} \\ \frac{\tau_{2,x} - \frac{t}{t_{ds}} U_{h,x}}{1 - \frac{t}{t_{ds}}} &= \frac{-\tau_{3,x} - (1 - \frac{t}{t_{ds}})(U_{h,x} + V_{h,x})}{\frac{t}{t_{ds}}} \end{aligned} \tag{18}$$

Now, equations (12), (14), (15) and (18) provide the 12 constraints needed to solve the system in the double support phase. Note that except (12), other equations are arbitrary choices to remove the redundancy. One might replace them with other policies for the same purpose. However, our simple assumptions preserve linearity and lead to a convincing match with human torque profiles, discussed in the next sections.

As mentioned earlier, 3LP switches to double support when the swing foot velocity becomes zero. This assumption, however, does not guarantee zero acceleration during the touchdown event. Therefore, a negligible discontinuity of torque and force profiles is unavoidable. In the simplest case, even preserving the continuity of horizontal GRF components lead to terms like $tx(t)$ which are linear, but difficult to solve analytically. With our specific linear transition rules, however, the profiles are almost continuous. Some discontinuities happen only in the transversal torques which are small in magnitude, demonstrated later in Figure.10.

In double support phase, the state variable consists of base positions only:

$$X^{ds}(t) = \left[X_{2,x}\ X_{2,y}\ x_{1,x}(t)\ x_{1,y}(t)\ X_{3,x}\ X_{3,y}\right]^T \quad (19)$$

while other vectors are the same as before. Again, we combine all equations and obtain a symbolic linear DAE system for the double support phase:

$$\frac{d^2}{dt^2}X^{ds}(t) = C_X^{ds}\,X^{ds}(t) + C_U^{ds}\,U + C_V^{ds}\,V + C_W^{ds}\,W + C_d^{ds}\,d \quad (20)$$

where constant matrices C^{ds} merely depend on system parameters (refer to Appendix.I for further details). Defining the full state vector $Q(t)$ and the constant vector R as before, we can obtain a similar system of closed form solutions as:

$$Q^{ds}(t) = A^{ds}(t)\,Q^{ds}(0) + B^{ds}(t)\,R \quad (21)$$

where the time-dependent transition matrices $A^{ds}(t)$ and $B^{ds}(t)$ describe state evolution over time. Note that since X_2 and X_3 are constant here, the matrix $A^{ds}(t)$ is partially diagonal with unit elements, keeping feet positions constant. The transition matrices have the following simple structure:

$$A^{ds}(t) = \sum_{i=1}^{4} A_i^{ds}\gamma_i^{ds}(t)$$
$$B^{ds}(t) = \sum_{i=1}^{4} B_i^{ds}\gamma_i^{ds}(t) \quad (22)$$

where $\gamma_i^{ds}(t) = e^{w_i^{ds}t}$ for $i = 1..2$, $\gamma_3^{ds}(t) = 1$ and $\gamma_4^{ds}(t) = t$. The two scalars w_i^{ds} are replicated square roots of the eigenvalues associated with the non-zero part of C_X^{ds} matrix.

Full stride

Having state transition matrices for both phases, we can now find closed form equations for the full stride phase:

$$Q(t) = A(t)\,Q(0) + B(t)\,R \quad (23)$$

where t denotes the time from the beginning of the full stride phase (= beginning of the double support) and $Q(t) \in \mathbb{R}^{12}$ is defined as:

$$Q(t) = \left[X(t)^T\ \dot{X}(t)^T\right]^T \quad (24)$$

and $X(t) \in \mathbb{R}^6$ is:

$$X(t) = \left[X_{2,x}(t)\ X_{2,y}(t)\ x_{1,x}(t)\ x_{1,y}(t)\ X_{3,x}\ X_{3,y}\right]^T \quad (25)$$

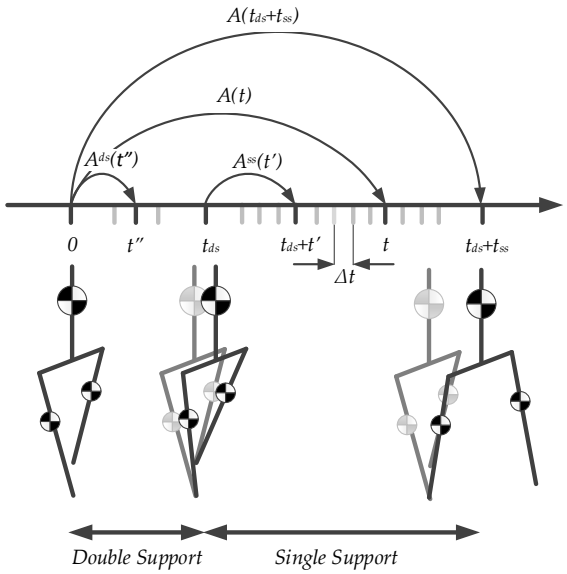

Figure 3. Demonstration of transition matrices on a time axis. Δt represents arbitrary time duration that could be as small as a control tick. Thanks to linearity, one can easily find exact transition matrices for Δt as well which could be used for visualization and control purposes. Otherwise, the matrix $A(t)$ is enough for gait generation.

The transition matrix $A(t)$ is defined as:

$$A(t) = \begin{cases} A^{ds}(t) & t \le t_{ds} \\ A^{ss}(t - t_{ds})A^{ds}(t_{ds}) & 0 < t - t_{ds} \le t_{ss} \end{cases} \quad (26)$$

and $B(t)$ is:

$$B(t) = \begin{cases} B^{ds}(t) & t \le t_{ds} \\ A^{ss}(t - t_{ds})B^{ds}(t_{ds}) + B^{ss}(t - t_{ds}) & 0 < t - t_{ds} \le t_{ss} \end{cases} \quad (27)$$

Note that we have used parameters t_{ss} and t_{ds} to calculate transfer matrices. The variable t_{ds} is crucial for double support calculations, though t_{ss} only determines the rate of time-increasing input components (V) in the single support. Therefore, one can easily scale t_{ss} and V such that the ratio remains constant in (6). The duration of a full stride phase is defined as $t_{stride} = t_{ds} + t_{ss}$. Figure.3 provides a demonstrates of all transition matrices and timing variables in a full stride phase.

So far in this section, we have found transition matrices for the system and defined a full phase, consisting of a double support followed by a single support. We have also formulated matrices such that they are very fast for online calculation. The matrix $A(t)$ is used to find the time evolution of our system, especially until the end of a full stride phase where $t = t_{stride}$. In the next section, we are going to find different open-loop periodic gaits based on the type of actuation desired.

Periodic gaits

Although various types of symmetric and asymmetric gaits can be generated (Rummel et al. 2010), in this paper, we only focus on symmetric gaits observed in normal human

walking. In other words, given timing specifications, we find a space of different vectors that produce symmetric gaits. Each of these vectors contains initial conditions and constant inputs. The concept of symmetry could be encoded in a single matrix along with the constraint of zero foot velocity at the end of the stride.

Consider the vectors $Q(t)$ and $X(t)$ in (24) and (25) respectively. Indeed, zero-velocity constraints imply:

$$\begin{aligned}\begin{bmatrix}X_{3,x}(t) & X_{3,y}(t)\end{bmatrix}^T &= const, \quad 0 \le t \le t_{stride}\\ \begin{bmatrix}\dot{X}_{3,x}(0) & \dot{X}_{3,y}(0)\end{bmatrix}^T &= 0\\ \begin{bmatrix}\dot{X}_{2,x}(0) & \dot{X}_{2,y}(0)\end{bmatrix}^T &= 0\\ \begin{bmatrix}\dot{X}_{2,x}(t_{stride}) & \dot{X}_{2,y}(t_{stride})\end{bmatrix}^T &= 0\end{aligned} \tag{28}$$

The first constraint is automatically satisfied by construction of matrices $A^{ss}(t)$ and A^{ds} where we assumed stationary stance foot (and thus zero acceleration). The other three constraints shall be satisfied in finding periodic gaits.

After a full stride phase, contact positions are exchanged by applying the matrix $T \in \mathbb{R}^{12\times12}$ to the vector $Q(t_{stride})$ where velocities are yet unchanged:

$$T = \begin{bmatrix}T_X & 0\\ 0 & I_{6\times6}\end{bmatrix} \tag{29}$$

where $T_X \in \mathbb{R}^{6\times6}$ is defined as:

$$T_X = \begin{bmatrix}. & . & . & . & 1 & .\\ . & . & . & . & . & 1\\ . & . & 1 & . & . & .\\ . & . & . & 1 & . & .\\ 1 & . & . & . & . & .\\ . & 1 & . & . & . & .\end{bmatrix} \tag{30}$$

To implement the symmetry concept, we define relative difference vectors between the base, swing foot, and stance foot positions. These vectors could be extracted from $Q(t)$ by the following matrix $M \in \mathbb{R}^{12\times12}$:

$$M = \begin{bmatrix}M_X & 0\\ 0 & M_{\dot{X}}\end{bmatrix} \tag{31}$$

where 0 and I are zero and identity matrices. Sub-block are also defined as:

$$\begin{aligned}M_X &= \begin{bmatrix}-1 & . & 1 & . & . & .\\ . & -1 & . & 1 & . & .\\ . & . & 1 & . & -1 & .\\ . & . & . & 1 & . & -1\end{bmatrix}\\ M_{\dot{X}} &= \begin{bmatrix} & & & I_{6\times6} & & \\ 1 & . & . & . & . & .\\ . & 1 & . & . & . & .\end{bmatrix}\end{aligned} \tag{32}$$

where M_X extracts difference vectors from the state vector and $M_{\dot{X}}$ is used to constrain swing foot velocities to zero. Comparing the difference vectors before and after a symmetric full stride, in the sagittal plane, components are equal, and in the lateral plane, they are opposite. Besides, we have to encode velocity constraints of (28) as well. So, we define a matrix $S \in \mathbb{R}^{12\times12}$:

$$\begin{aligned}O = diag(\quad & [1,-1,1,-1,0,0,\ ...\\ & 1,-1,0,0,1,1]\qquad)\end{aligned} \tag{33}$$

where symmetry conditions are applied to the difference vectors and the base velocity while feet velocities are forced to zero. Now, consider in initial condition vector $Q(0)$ and inputs R. The state at the end of a full stride is:

$$Q(t_{stride}) = A(t_{stride})Q(0) + B(t_{stride})R \tag{34}$$

Applying contact exchange matrix, the initial state $Q'(0)$ for the next phase is:

$$Q'(0) = TQ(t_{stride}) \tag{35}$$

The difference vectors extracted from $Q(0)$ and $Q(t_{stride})$ should satisfy symmetry conditions while initial and final foot velocities in $Q(0)$ and $Q(t_{stride})$ should be zero. One can write these conditions as:

$$MQ(0) = OMQ'(0) \tag{36}$$

Now, for a general vector of initial conditions and actuation parameters packed together:

$$Y = \begin{bmatrix}Q^T(0) & R^T\end{bmatrix}^T \tag{37}$$

the following equation should hold if Y represents a symmetric periodic gait:

$$DY = 0 \tag{38}$$

where:

$$D = \begin{bmatrix}-M + OMTA(t_{stride}) & OMTB(t_{stride})\end{bmatrix} \tag{39}$$

The matrix $D \in \mathbb{R}^{12\times25}$, in fact, compares the difference vectors before and after a full stride phase while forcing feet velocities to zero. Note that apart from state vectors, the hip and contact torques U and V, the disturbance vector W and the variable d are considered here. However, it is meaningless in practice to consider a periodic gait with constant external disturbance. Initial contact positions X_3 would be set to zero to avoid redundant null space dimensions.

Remember that in the previous section, there were two variables to decide: t_{ss} and t_{ds}. In this section, we find various types of gaits by selecting different combinations of actuation and timing variables. We do so by considering the matrix D which is, in fact, a function of timing variables. Any periodic solution (a vector containing initial states and actuation inputs) should lie in the null space of the D matrix. In other words, solution manifolds are found by combining different null vectors of the matrix D. A solution contains initial states and actuation parameters where available actuators are swing hip and stance ankle torques (in sagittal and lateral directions), in constant U and time-increasing modes V. Note that only columns attributed to non-zero values in the solution vector are selected. In other words, we normally exclude columns related to contact positions X_3 and disturbances W.

In the rest of this paper, we use human-like body parameters for numerical simulations, where mass distributions and geometries are taken from (De Leva 1996). Table.2 lists these parameters for two adult-size and kid-size models, used further in this paper.

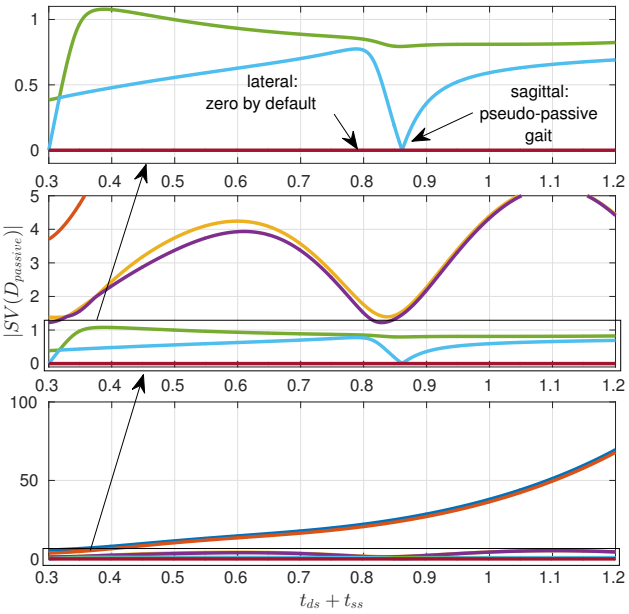

Figure 4. Absolute singular values of $D_{passive}$ versus t_{stride}, plotted for an adult-size model. In these plots, we fix the double support time $t_{ds} = 0.3$s and only change t_{ss}. It is notable that around $t_{stride} = 0.86$s, the system shows zero singular values which correspond to a null space containing an infinite number of periodic solutions. These solutions are all without swing hip or stance contact actuation referred to as pseudo-passive gaits.

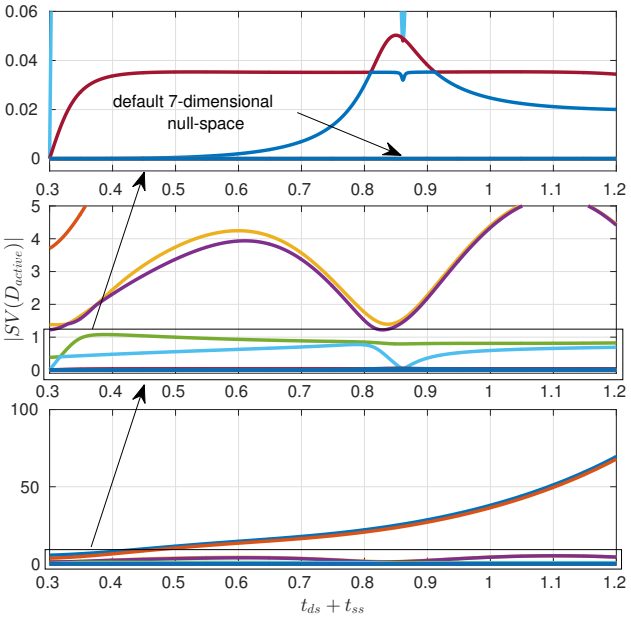

Figure 5. Absolute singular values of the matrix D_{active} with respect to the stride time t_{stride}, plotted for an adult-size model. In these plots, we have fixed the double support time $t_{ds} = 0.3$s. It is notable that the system does not show a unique zero singular value anymore. However, there are always 7 default zero singular values that can produce gaits for any choice of t_{stride}. These gaits are indeed actuated with arbitrary swing hip or stance ankle torque profiles.

Pseudo-passive gaits manifold

First, we would like to know whether the system has any pseudo-passive walking pattern or not. By pseudo-passive, we mean a gait in which swing hip and stance contact torques are zero. The term pseudo indicates that in the stance hip, the actuators might produce or dissipate power and the system is not strictly passive. This term also reflects the fact that in our linear model, the legs are stretched or shortened by prismatic actuators, as part of the model construction. For pseudo-passive gaits, we remove columns associated to X_3, U, V and W in D and obtain a reduced matrix $D_{passive} \in \mathbb{R}^{12\times 11}$. Figure.4 shows absolute singular values of $D_{passive}$ over time.

One can clearly see that there is a time $t_{stride} = t_{relax} = 0.86$s where the system shows an additional zero singular value. t_{relax} can be found by a simple root-finding algorithm. This singular value refers to sagittal direction while the other singular value (which is always zero) refers to lateral direction. We can simply calculate corresponding singular vectors of $D_{passive}$ and find a null space manifold. Note that there is only one lateral solution as the value of d should be ± 1. However, the solution in the sagittal plane can be scaled by any arbitrary positive or negative value to obtain different modulated speeds. Therefore, the manifold of pseudo-passive compass gaits, in this case, is only 1-dimensional. A demonstration of normal pseudo-passive compass gaits can be found in Figure.6. From Figure.4 also, we simply conclude that for any stride time other than t_{relax}, the system cannot demonstrate pseudo-passive gaits.

Model	adult-size	kid-size	unit
Total mass	70	30	kg
Body length	1.7	1.0	m
z1	0.89	0.52	m
z2	0.32	0.19	m
z3	0.36	0.22	m
m1	45.7	19.6	kg
m2=m3	12.15	5.2	kg
$w/2$	0.1	0.06	m

Table 2. Parameters for adult-size and kid-size models used in simulations.

Actuated gaits manifold

In this part, we are going to find manifolds of motion which can benefit from swing hip actuation and CoP modulation as well. These inputs are of course containing constant and time varying components for both sagittal and lateral dynamics, as discussed in the previous section. With these inputs, we can pump energy into the swing leg and brake at the end of the phase to produce faster swing motions. We can also apply contact torques which modulate the CoP and resemble the fact the CoP in human goes forward from the heel to the toes during the swing phase. Here we only remove columns associated to X_3 and W in D and obtain a reduced matrix $D_{active} \in \mathbb{R}^{12\times 19}$. The corresponding absolute singular values are shown in Figure.5 over time.

Surprisingly, the system does not have a distinct zero singular value at t_{relax} like before. However, it has 7 zero singular values that produce a larger null space at any given stride time t_{stride}. The corresponding actuated gait manifold is not 7-dimensional however. The variable d should always

be ± 1, reducing the total dimensions to 6. Besides, one can also choose active actuators and the desired speed to reduce the dimensionality further and find a unique solution.

As demonstrated in pseudo-passive gaits, at t_{relax}, $D_{passive}$ has a certain 2-dimensional null space. Now what if we calculate a 7-dimensional null space using t_{relax} and D_{active} instead of $D_{passive}$? Could we still find a pseudo-passive gait out of this larger null space? In fact, it is possible, even though no distinct zero singular value is observed in Figure.5. The reason is that the rank of actuation space at t_{relax} is equal to 5 in the 7-dimensional null space manifold of D_{active}. This means if we constrain all of them to zero for pseudo-passive walking, we only lose 5 ranks. The other 2 ranks could still be dedicated to the variable d and the desired speed, like before. So, the null space manifold of actuated gaits already encompasses the one for pseudo-passive gaits and we do not need to calculate them separately. In the next subsection, we are going to show a few examples of walking gaits, using these null spaces.

Numerical examples

In addition to the pseudo-passive gait which has a certain timing t_{relax}, we are going to show other same-speed gaits with different timings and actuation patterns. From the singular value analysis, we have 7 singular vectors $n_i, 1 \leq i \leq 7$ for the matrix D_{active}. Each of these vectors have similar dimensions with Y in (37), consisting of an initial state, with the contact point (X_3) at origin, a resting swing foot ($\dot{X}_2 = 0$), a certain actuation pattern (encoded in U and V) and no disturbance ($W = 0$) of course. We pack them together in a matrix $N = \begin{bmatrix} n_1 & n_2 & \dots & n_7 \end{bmatrix}$. We also select a smaller yet more human-like choice of $t_{ds} = 0.1$s (Cappellini et al. 2006), and $t_{ss} = 0.6028$s calculated by the pseudo-passivity root finding procedure. The choice of speed will be $v_{des} = 1$m/s.

Given the constant matrix N, we want to find a vector of coefficients $\delta = \begin{bmatrix} \delta_1 & \delta_2 & \dots & \delta_7 \end{bmatrix}^T$ that combine the columns in N and produce unique solutions. We consider minimizing squared torques as an estimate of the mechanical power. The quadratic minimization is formulated as:

$$\begin{aligned} &\underset{\delta,U,V}{\text{minimize}} \;\; U^T U + V^T V \\ &\text{s.t.} \\ &\begin{bmatrix} S_{X_{2,x}} \\ S_U \\ S_V \\ S_d \end{bmatrix} N\delta = \begin{bmatrix} -v_{des} \times t_{stride} \\ U \\ V \\ \pm 1 \end{bmatrix} \end{aligned} \tag{40}$$

where $S_{X_{2,x}}$ selects the row corresponding to the sagittal swing foot position ($X_{2,x}$), S_U and S_V correspond to the constants U and V and S_d corresponds to the constant d. The specific way of encoding v_{des} in the optimization moves the initial swing foot position backward to find gaits with an average velocity equal to v_{des}. Note that the equality constrained quadratic optimization of (40) has, in fact, a closed form solution and there is no need to solve it iteratively.

Now consider the following scenarios:

- **Pseudo-passive walking:** which is calculated as mentioned earlier. In this gait, the hip and ankle torques are all zero.
- **Long double support:** in this gait, we enforce ankle torques to zero by adding more constraints to the optimization:

$$\begin{bmatrix} S_{U_a} \\ S_{V_a} \end{bmatrix} N\delta = 0 \tag{41}$$

  where S_{U_a} and S_{V_a} select rows corresponding to the stance ankle torques. Keeping the same t_{stride}, we double t_{ds} and decrease t_{ss} accordingly. Note that now, the walking cannot be pseudo-passive anymore. The optimization, therefore, finds nonzero hip torques to produce the same speed and stride length.
- **Stage walking:** here, we constrain the ankle torques to zero like before. Instead of optimizing the hip torques, however, we optimize lateral velocities in the cost function. In this case, the biped walks on a straight line without lateral bounce.
- **CoP modulation:** given the length of the feet, the total weight and the timing of single support, we can calculate a constantly increasing ankle torque $\frac{t}{t_{ss}}\tau_{CoP}$, acting in the sagittal plane to move the CoP forward. In this scenario, we force the time-increasing sagittal component of the ankle torques to τ_{CoP} (and other components to zero) by adding the following constraints to the optimization in (40):

$$\begin{bmatrix} S_{U_a} \\ S_{V_a} \end{bmatrix} N\delta = \begin{bmatrix} 0 & 0 & \tau_{CoP} & 0 \end{bmatrix}^T \tag{42}$$

  The result is a gait with time-increasing ankle torque profiles and minimal hip actuation.
- **LIP-like:** in this case, keeping the original timing, we change the model of the robot. We transfer most of the weight of each leg to the torso, and also move the three masses closer to the pelvis by decreasing h_2 and h_3. Again, we disable all ankle torques as well.

The 3D geometry of resulting gaits are shown in Figure.7 while a detailed diagram of each stride is shown in Figure.6. The accompanied Multimedia Extension 1 demonstrates different features of 3LP while Multimedia Extension 2 shows movies of the five previously mentioned scenarios. It can be concluded from the Figure.7 that changing different parameters does not have a major effect on the overall geometry of walking. However, since it is important to match dynamics of the full model, we investigate dynamic properties of these walking scenarios as well.

Although CoM trajectories look similar in Figure.7, they have very different characteristics regarding velocity variations, shown in Figure.8. The LIP-like model shows a significant variation in the sagittal velocity. It is not so obvious how swing and torso dynamics affect this motion at first glance. By torso dynamics, we mean the torques required by the stance hip to keep the torso always upright. These torques are not necessarily zero since the pelvis has nonzero accelerations. Therefore, torso-balancing hip torques can affect the CoM motion considerably, especially since the torso is relatively heavy. Moreover, although the swing foot has a smaller weight compared to other parts of the body, it can be seen from Figure.9 that the swing leg has relatively large velocities during single support. Such motion increases the kinetic energy quadratically and

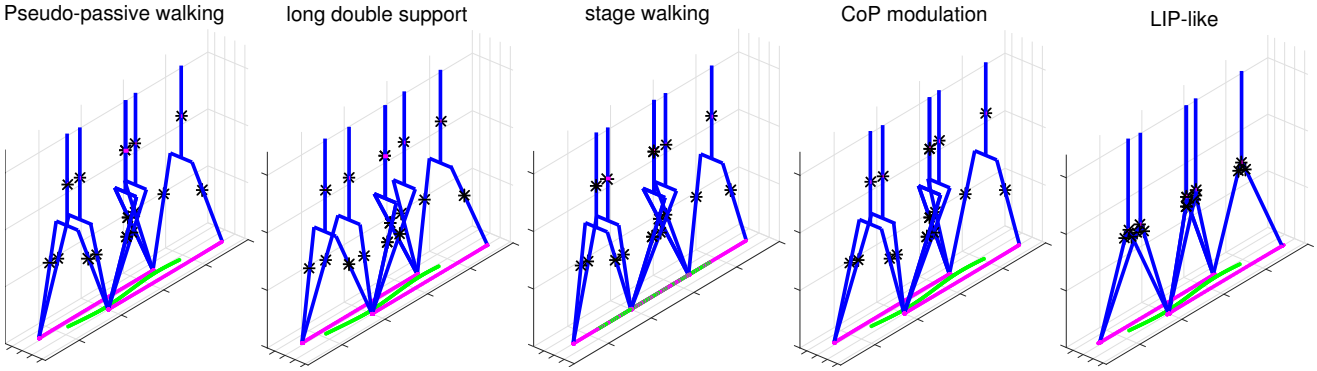

Figure 7. Snapshots of different walking scenarios at 1m/s and approximately 1.5step/s. These snapshots are taken in phase switching moments. Feet trajectories are plotted along with the projection of the CoM trajectory on the ground. In pseudo-passive walking, there is no actuation. However, one can clearly see that the model can produce CoM trajectory, lateral bounces, and swing motions. In the long double support case, the motion is geometrically quite similar. Stage walking produces no lateral bounce by using proper hip torques to let the model step on a single straight line only. On the real robot, however, one should avoid self-collision, and this motion is thus infeasible. CoP modulation also leads to a geometry similar to pseudo-passive walking, though CoM trajectory (the green line on the ground) starts a bit further from the trailing leg. The influence of CoP modulation is mainly reducing variations in the sagittal CoM speed (Figure.8). Finally, the motion of LIP-like model is rather similar to the pseudo-passive case, but with higher CoM speed variations (Figure.8). In this case, we enforce lateral footstep distances to mimic other scenarios, since the pelvis width is minimal. All corresponding walking movies could be found in Multimedia Extension 2.

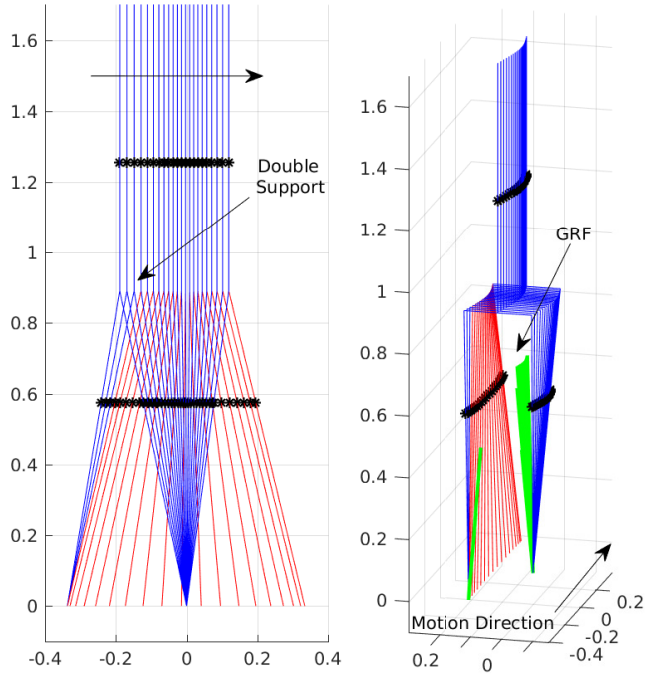

Figure 6. A detailed demonstration of a full stride phase in pseudo-passive walking where snapshots are taken every 30ms. Black arrows show the direction of motion, and the swing leg is shown in red. In this figure, lateral bounces could be seen on the right while velocities can be inferred from the snapshots on the left. The swing leg speeds up and slows down during a stride phase while the torso has minimum speed when the swing foot is at maximum speed. It can also be observed that the swing foot approximately follows a straight line while the swing hip bounces laterally.

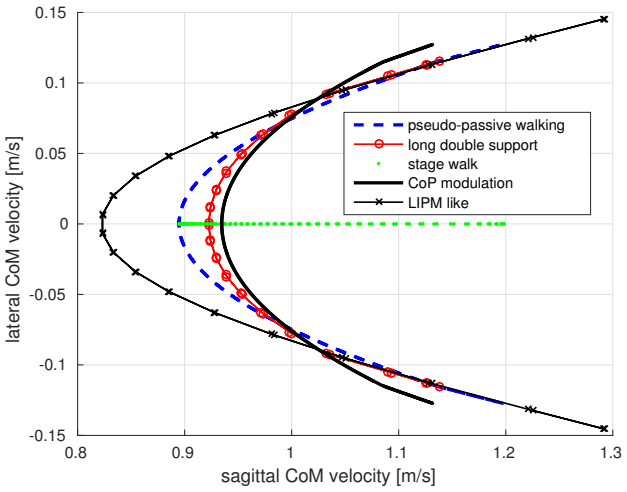

Figure 8. Sagittal vs. lateral CoM velocity trajectories for different scenarios discussed. Note that the LIP-like model produces significant sagittal variations. The pseudo-passive gait shows moderate variations, however, indicating that swing and torso dynamics clearly reduce these variations. Long double support also reduces variations in both directions. By modulating the CoP, although lateral motions remain similar to the pseudo-passive gait, sagittal variations reduce even more, and the motion becomes smoother. Finally, one can see that the stage walking has no lateral motion compared to the other gaits. In general, increasing the double support duration and CoP modulation both have a similar smoothing effect on CoM velocities. However, this does not induce any argument on energy efficiency.

therefore results in a significant workflow. In our model, we have described these effects in a simplified and linear fashion, yet capturing important couplings between the three pendulums.

Taking a closer look at Figure.8 reveals that even maximal CoP modulation still does not change velocity profiles considerably. This means the difference between pseudo-passive and LIP-like walking is way larger than that between pseudo-passive and CoP-modulated walking. In other words, CoP authority can at most convert the pseudo-passive gait to the CoP-modulated gait. The available CoP authority

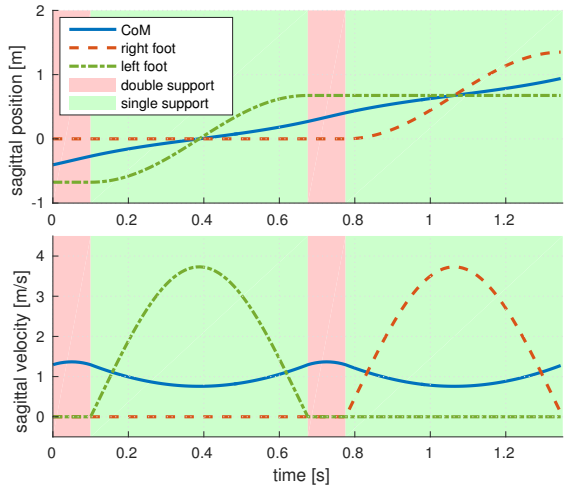

Figure 9. CoM and feet positions plotted together with velocities over a 2-stride motion. The average speed is set to 1m/s, the frequency is about 1.5step/s and the pseudo-passive gait is used to obtain these trajectories. It can be observed that maximum foot velocities are up to three times larger than the average speed of the CoM. Despite a smaller mass, therefore, the swing leg can have a considerable kinetic energy.

is hardly enough to convert the pseudo-passive gait to LIP-like gait, and this gap increases substantially at faster walking speeds. Although here the speed is moderate, we can easily infer that LIP as a template model can only operate in a very limited range of walking speeds. Remember that in fact an inverse dynamics or kinematics approach eventually realizes the template motion with the full model by exploiting all control authorities of the robot (including the CoP). This motivates therefore not to modulate the CoP in a template level and leave the control authority free for the underlying full-body controllers to mimic the template motion as precisely as possible.

In this section, we introduced an easy method to find manifolds of periodic motions without any numerical forward simulation of the system. Once these manifolds were found, we also showed how to find individual solutions, based on the type of actuation and timing desired. We only considered gaits with minimal hip torques here. However, to go further, we would like to investigate the effect of timing and walking speed as well. Such investigation reveals interesting energetic properties of 3LP, discussed in the next section.

Comparison with human data

Compared to LIP, the 3LP model is much more similar to human locomotion, because it describes falling dynamics, swing motion, torso balance, lateral stepping and double support features altogether. In addition to geometric similarities, we investigate ground reaction forces and joint torques to compare the underlying dynamics that result in such geometric similarity. For this purpose, regarding available data from human subjects (Eng and Winter 1995), we selected similar model parameters and timing, calculated periodic manifolds and found solutions with the same speed and CoP modulation pattern. The resulting trajectories are demonstrated in Figure.10 together with average human profiles. In the following, we discuss various similarities observed in this figure.

Sagittal dynamics

From the last column of Figure.10, one can observe a good match of hip extensor and ankle plantar flexor torques as well as Anterior-Posterior ground reaction forces. This is despite a relatively fast walking speed and large step sizes (about 80% of the leg length). Note also that the constant and time-increasing components of hip/ankle torques are roughly enough to describe major trends in human curves. Nonlinear profiles in 3LP are, however, related to the stance leg and those degrees of freedom which are not directly controlled by desired input torques. The LIP model does not have hip torques and produces larger A/P GRF, because of different CoM trajectories shown in the Figure.8.

Vertical GRF

By model construction, the CoM height is constant, and we do not expect two peaks in the vertical GRF profiles, similar to SLIP-based models (Rummel et al. 2010; Sharbafi and Seyfarth 2015). However, the general trapezoidal shape is preserved, thanks to our double support phase and its linear transition rules. Note that the LIP model can produce a similar profile too. The main consequence of a constant-height profile is walking with crouched knees which looks less human-like compared to many other template models listed in Figure.1.

Lateral dynamics

In 3LP, we only minimize hip/ankle torques to find a unique solution out of the large manifold of all symmetric periodic gaits. This minimization is not necessarily realistic and human-like, as it leads to wider lateral steps, more bouncing, and often larger transversal ankle torques. A better cost function on energy might produce more human-like gaits, although it is doubted in (Workman and Armstrong 1986) that optimal gaits merely depend on energy terms. There might be terms related to balancing performance as well, at least in lower speeds. In faster speeds also (like the human profiles demonstrated here (Eng and Winter 1995)), humans take closer steps laterally compared to our model.

In Figure.7), we see that 3LP keeps general trends like double peaks in the Medio-Lateral (M/L) GRF, but cannot precisely describe other torque profiles. Humans normally tend to step as close as possible to minimize lateral motions and energy (Kuo 1999) (Similar to stage walking in Figure.7). However, humans swing their foot over an arc shape to avoid self-collision. Such a fine motion is feasible in 3LP but requires a better objective function in (40). Note that the sagittal swing motion can influence lateral dynamics as well (Kuo 1999; Collins et al. 2005), possibly through transversal moments. This might be another reason for the discrepancy observed between different lateral curves since 3LP completely decouples the lateral and sagittal dynamics. In the LIP model, though, there is no pelvis included. However, we consider a gait with the same step-width as 3LP. Although LIP does not have hip torques, M/L GRF forces are yet similar to 3LP, shown in Figure.7.

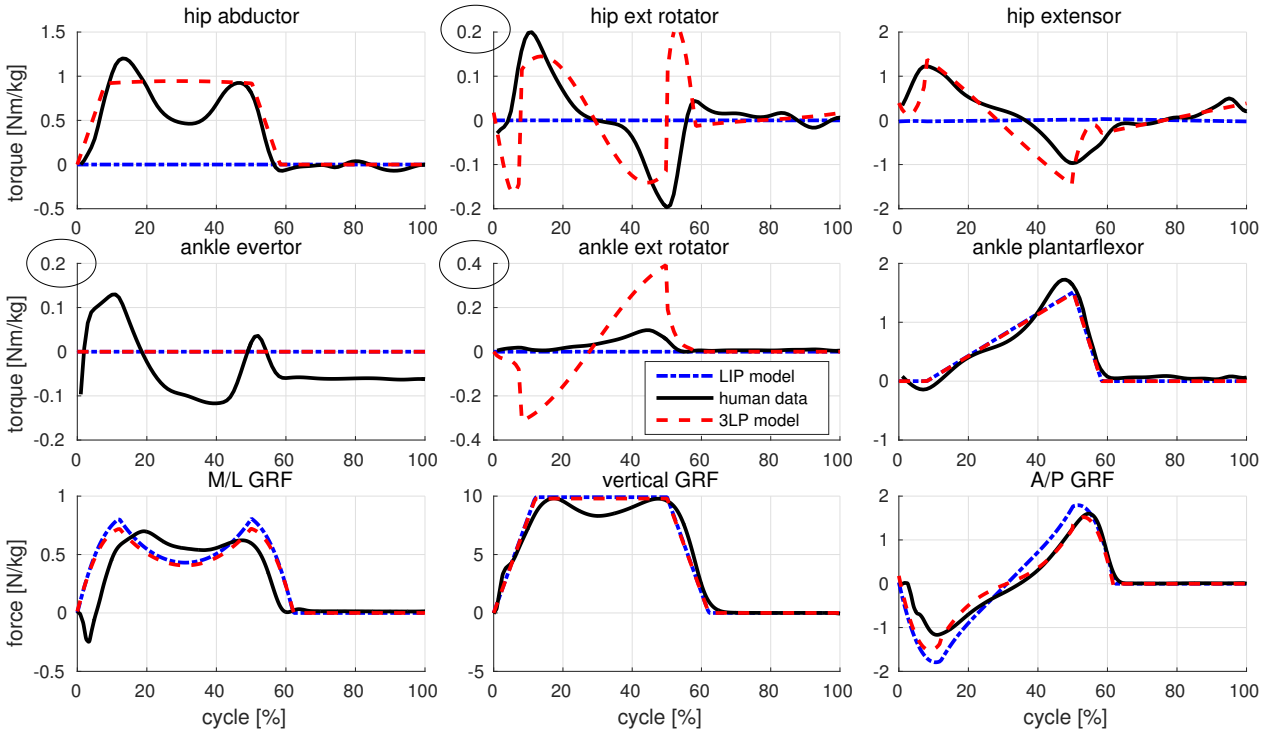

Figure 10. Comparing dynamic profiles of 3LP and LIP with normalized human data, taken from (Eng and Winter 1995). This data is for male subjects with average mass of 77.2kg and height of 1.8m, walking at 1.6m/s and 108steps/min. Here we use the same CoP modulation for both LIP and 3LP for better comparison. In these curves, we have demonstrated hip/ankle torques as well as ground reaction forces. Note that our model does not have any knee and we consider ankle torques to approximate contact wrenches. Most of the profiles in 3LP match the human data quite well, although lateral and transversal dynamics have some discrepancies. The LIP model is, however, unable to describe hip torques as it does not include swing and torso dynamics. It is also remarkable that our specific assumptions in (14), (15) and (18) move the discontinuity on variables with smaller magnitudes (shown with circles).

Transversal rotation torques

3LP preserves the general trend of transversal torques observed in human, but not matching precisely, especially in the ankle. One major reason is that arm motions, and pelvic rotations are not considered in the model. Another important reason is wider lateral steps in 3LP compared to human which require larger transversal moments. Note that transversal torques are needed to keep the torso upright and straight ahead during swing phase, compensating the moment produced by the swing leg. In LIP, however, since there is no pelvis and swing leg, we do not expect transversal torques.

Energetics

Apart from dynamics profiles, it is always interesting to investigate energy flow in the model and compare it with the human. Remember that one of the main motivations behind developing 3LP was to match humanoid dynamics as precise as possible in the template space. Such matching could be viewed from a power-flow perspective as well, inspired by the fact that humans can walk very efficiently. Compared to LIP, 3LP can additionally describe swing and torso dynamics which are important aspects of locomotion, especially at faster speeds. Since the pelvis has accelerations in sagittal and lateral directions, the whole upper-body requires nonzero hip torques to balance. Our model successfully encodes the influence of these torques on the horizontal motion.

Energy trade-offs: Although the mass of swing leg is relatively small, its peak velocity is about three times larger than the torso which has a heavier mass. Therefore, the peak kinetic energy of the swing leg is quite comparable with the torso. Such energy comes from both the accelerated pelvis where the swing leg is attached to and swing hip

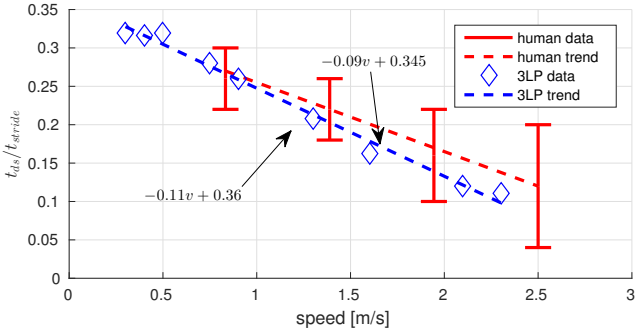

Figure 11. The optimal choice of double support ratio in 3LP versus human data (Cappellini et al. 2006), over normal walking speed-frequency curves reported in (Bertram 2005). In this figure, for each particular choice of speed and frequency, an optimization has found the optimum double support ratio by maximizing walking efficiency. Since the mass and body height of individual subjects were not reported, we used the average body mass 66kg and height 1.7m in (Bertram 2005). For both human and 3LP data, we also used a linear model to find the trends.

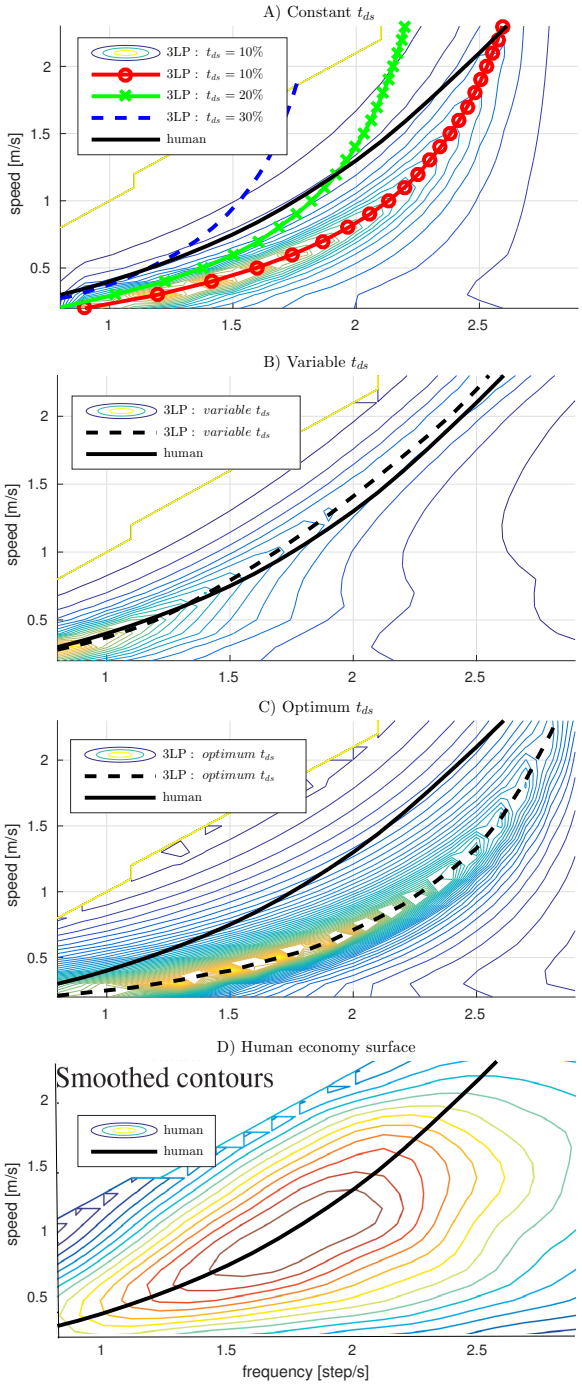

Figure 12. Efficiency (economy) of walking, i.e. the inverse of Cost of Transport (CoT) which is calculated as positive work on the CoM over a unit of distance traveled, normalized by body mass. Here, we set body mass to 66kg and body height to 1.7m with normal human-like mass distribution (De Leva 1996). A) Contours of 3LP-based walking efficiency, calculated for the choice of $\frac{t_{ds}}{t_{stride}} = 10\%$. Peaks for this double support ratio as well as other choices of 20% and 30% are plotted versus the optimal relations observed in human. 3LP can demonstrate a peak line, but not matching with human data. B) 3LP-based efficiency, using the double support ratio of (44). Now, 3LP can provide a roughly close prediction. C) Optimal walking efficiency, where for each choice of speed and frequency, an optimization finds the double support time ratio that maximizes the efficiency. Here, 3LP does not match human trends anymore. D) The smoothed contours of human walking efficiency, taken from (Bertram 2005).

torques that can modulate swing dynamics. In a trade off with falling dynamics, this phenomenon can explain optimal speed-frequency relations observed in the metabolic cost of human walking (Bertram 2005). Although 3LP does not include many important walking determinants like heel-toe motions, knee flexions and CoM excursions (Inman et al. 1953), surprisingly, it can capture the main optimality trend in human walking.

Comparison method: We consider two parameters of locomotion: stepping frequency and forward speed. Similar to (Bertram 2005), we calculate the efficiency of walking (called economy in the original paper) for different speed-frequency combinations. Efficiency is defined as the inverse of the cost of transport, which is the total energy consumed per unit of mass, per unit of distance traveled. There are many ways to calculate such mechanical power in our model. In fact, 3LP does not simulate muscles and the exact geometry of a human and thus, it is unable to precisely reconstruct the human efficiency surface based on the metabolic cost. However, by integrating the positive part of the mechanical power, we can approximate a portion of this energy which still plays a major role in the overall energy landscape according to (Anderson and Pandy 2001). We are not able to model other costs like muscle activation, maintenance and shortening heat rates since we do not have muscles in 3LP.

Fixed double support time: We calculate the net positive work divided by the total mass over a grid of different speed-frequency combinations that cover slow to fast walking gaits (Bertram 2005) . Figure.12A demonstrates corresponding efficiency contours for the choice of $\frac{t_{ds}}{t_{stride}} = 10\%$. It is surprising that the model shows a peak line within the range of speed-frequencies explored in (Bertram 2005). Such peak, in fact, demonstrates the trade-off between swing and falling dynamics. The former increases in higher frequencies, since more energy is pumped into the swing leg and taken out by braking at the end of the swing phase (Doke et al. 2005). The latter, however, increases by step-size which results in larger CoM velocity variations.

We repeated the same process for two other choices of double support time: 20% and 30%. The resulting peak lines are demonstrated in Figure.12A as well as the optimal trend of human data (shown in black), taken from (Bertram 2005) (the case of constrained speed). Here we use the same average mass (66kg) and height (1.7m) of human subjects in (Bertram 2005) as well as average mass distributions reported in (De Leva 1996). Although 3LP is successful in identifying the trade-off, using the choice of constant double support time ratio, it fails to match the human data.

From Figure.12A, it can be hypothesized that in slow speeds, humans have larger double support ratios compared to higher speeds. Measurements of this quantity from recorded human gaits verify this hypothesis, suggesting a linear relation between the double support ratio $\frac{t_{ds}}{t_{stride}}$ and the walking speed v:

$$\frac{t_{ds}}{t_{stride}} = -0.09\, v + 0.345 \tag{43}$$

This relation gives a ratio of 27% at $v = 0.8$m/s and 12% at $v = 2.5$m/s, close to our three initial conjectures. Does 3LP predict such relation too?

Human-like double support time: We took the optimal speed-frequency trend line in human data (Bertram 2005) (shown in Figure.12 A with black color) and performed a simple optimization to find the choice of $\frac{t_{ds}}{t_{stride}}$ which maximizes walking efficiency in each combination of walking speeds and frequencies. Since we did not have access to anatomical parameters of individual subjects in (Bertram 2005), we performed optimization for the average body mass (66kg) and height (1.7m) reported. The resulting curves are shown in Figure.11 for both human and 3LP, where a line fitted to 3LP values is found as:

$$\frac{t_{ds}}{t_{stride}} = -0.11\, v + 0.36 \tag{44}$$

This line is indeed very similar to the optimal trend line in human data, although it predicts shorter double support times in faster speeds. Repeating the same grid search of Figure.12A with the particular choice of double support time in (44), we obtain Figure.12B.

Optimal double support time: If we do not limit the optimization to the optimal trend line of human data and perform it everywhere for all combinations of speeds and frequencies, 3LP finds a different trend line, shown in Figure.12C. This is expected, however, since our simplifying linear assumptions in the double support phase can only approximate the real curves in Figure.10 to some extent. To predict optimal trends in human data without using any information about human walking, we need more complex double support formulations and better optimality criteria. The results shown in Figure.12 are very promising and important, despite the fact that:

- No impact or push-off is considered.
- CoM height is constant.
- No foot clearance is modeled.
- Heel-toe motions and knee flexions are not included.
- The torso has no rotation in any direction.
- Weight support cost on the stance leg is not considered.
- Walking-independent metabolic cost components are not modeled.

Therefore, although the optimal speed-frequency trend is roughly predicted in Figure.12B, the overall 3LP-based efficiency surface is not matching the human data shown in Figure.12D. Linear models are conventionally expected to be a linearization of the actual non-linear system, performing better in near-stance (small step-size) conditions, where the geometry of 3LP is more close to the actual system. 3LP does not model heal-toe-knee motions and intrinsically simplifies them with an extensible prismatic actuator. However here, it appears to demonstrate a similar mechanical energy flow, even with large step sizes. In future works, we would explore other components of walking energy, keeping 3LP as a core model. Inclusion of other costs might reconstruct the actual human efficiency surface more precisely.

Conclusion

Compared to most of other template models listed in Figure.1, our proposed model considers swing and torso dynamics in a linear formulation. On the other hand, it is computationally similar to LIP which is vastly used in the literature to control humanoids over a range of relatively slow walking speeds (Sakagami et al. 2002). Nonlinear models are also popular in controlling simpler robots (Collins et al. 2005), but again over a limited range of speeds.

Template models describe major dynamics of the robot in an abstract way used for motion analysis or synthesis, probably in a hierarchy with more complex full models. In such control paradigms, it is important to keep computational costs as minimal as possible, favoring future prediction. On the other hand, template models should match the full models dynamically. 3LP can describe many features of human walking, and consequently, it is more precise for controlling humanoids, compared to many other single-mass models. The energy flow in 3LP is also more similar to the human, providing more natural motions for humanoids which have similar anthropomorphic features.

In 3LP, the pelvis width parameter has a linear effect on the lateral motion. This parameter is used to find lateral ankle/hip torques and to determine a natural lateral foot placement. This is compared to many of other methods like (Faraji et al. 2014) where the two feet are forced to be apart to avoid self-collision. In the literature, the timing and footstep locations are imposed without enough knowledge of internal dynamics. In our model, however, since swing dynamics is included and a zero final velocity is assumed for the feet, natural periodic gaits automatically come out of equations. The assumption mentioned relieves the need to calculate impact forces and determines the timing and periodicity conditions as well.

3LP can predict human walking profiles quite well, even in relatively fast speeds where the linearity assumption might not be realistic. Although IP-based models can demonstrate CoM excursions quite well, a nonlinear nature makes them less suitable for highly complex robots that require online planning. There are more advanced versions of IP-based models in the literature, including torso and swing dynamics. However again, nonlinear equations cannot be used in a per-time-step MPC control. The proposed model is based on a reasonable trade-off between geometric and dynamic matching, favoring fast computation properties.

We showed that 3LP could also describe the exchange of energy between swing and falling dynamics, despite a constant CoM height. We would like to mention that the vertical excursion of CoM, even in a very fast walking gait at 2m/s is still about 5cm (Gard et al. 2004) which is quite negligible compared to a step-size of about 1m (pelvis excursion is about 7cm however). CoM excursion depends on step-size which does not increase linearly with the walking speed. Humans increase the frequency as well, which in consequence affects swing dynamics and demands more energy from the hip muscles.

We did not set up control frameworks in this paper. Rather, we focused on biomechanical analysis and similarities to human locomotion that can be inspiring for generating more precise abstract plans, used to control humanoid robots. In brief, 3LP provides:

+ Swing dynamics.
+ Torso balancing torques.
+ Double support phase.
+ Hip/ankle actuation possibilities.

+ Natural lateral motion.
+ Natural periodic gaits.
+ Pseudo-passive compass gait.
+ Computational advantages.
+ Possibility to consider hip torque limits.
+ Optimal speed-frequency relation similar to human.

Despite limiting factors such as:

- Constant CoM height.
- Flat vertical GRF profiles.
- Stretched legs.
- No steering capabilities yet.
- No arm motion.
- No torso pitch/roll DoF.

3LP can be extended to have two more degrees of freedom for the torso. It can also include quadratic actuation terms to produce more accurate torque profiles. It should be noted that without pelvis, steering is still possible as demonstrated in our previous work (Faraji et al. 2014) which is based on LIP. Steering makes 3LP nonlinear, but one can compromise the lateral motion and let inverse dynamics find proper actuation patterns. Without the pelvis in 3LP, one actually needs to impose the lateral bouncing as we did in the LIP-like scenario. An important role of pelvis is, therefore, to produce a natural lateral motion which automatically emerges from the optimization of (40). This makes the model more generic without the need to impose the lateral bouncing. Note that the natural step width is not easy to determine, since it depends on the leg length, stepping frequency and available ankle torques.

It is worth mentioning that an imposed step width which is similar to the natural step width (found when including the pelvis) might not produce very different GRF profiles. This is induced from Figure.10 by comparing GRF profiles of the LIP-like scenario and the full 3LP model. As a result, one can easily remove the pelvis and allow for steering with the cost of imposing the step width. This can be realized by finding a natural step width with the pelvis and then imposing it in another version of 3LP which does not have the pelvis anymore. The second model remains natural (in terms of GRF), linear and of course suitable for producing steering motions.

In future work, we are going to replace LIP with 3LP in our MPC-based control framework (Faraji et al. 2014). 3LP can be used in both state estimation and planning levels. It can possibly exchange information about the CoM or the feet with the full model. Dynamic equations of 3LP can, therefore, predict future states in a MPC framework or help to filter sensory noises by Kalman filtering. The linear equations of 3LP can indeed provide a non-periodic formulation of the system as well, where footsteps might act as inputs to the system instead of the hip torques. This reformulation is similar to planning footsteps in MPC (Faraji et al. 2014) or Capturability frameworks (Koolen et al. 2012).

Among all advantages offered by 3LP, we favor its capability to produce more natural motions. In this regard, we can expect our inverse dynamics layer to track the template model more precisely and therefore, being able to produce more human-like motions. Including torso and swing dynamics in template models make them computationally more complicated, but closer to reality. In the literature, complex models are mostly used for offline trajectory generation. In 3LP, however, we partially include these additional dynamic effects while keeping the model yet suitable for online control and future prediction. The focus of this paper was to introduce the model and to explore different capabilities. In future, we integrate it with our hierarchical walking controller to achieve more dynamic motions. This paper is accompanied with two multimedia extensions, demonstrating general features of 3LP together with the five gait scenarios discussed. All codes used in this article are available online at http://biorob.epfl.ch/page-99800-en.html.

Acknowledgements

This work was funded by the WALK-MAN project (European Community's 7th Framework Programme: FP7-ICT 611832).

References

Frank C Anderson and Marcus G Pandy. Dynamic optimization of human walking. *Journal of biomechanical engineering*, 123 (5):381–390, 2001.

Fumihiko Asano, Masaki Yamakita, Norihiro Kamamichi, and Zhi-Wei Luo. A novel gait generation for biped walking robots based on mechanical energy constraint. *Robotics and Automation, IEEE Transactions on*, 20(3):565–573, 2004.

John EA Bertram. Constrained optimization in human walking: cost minimization and gait plasticity. *Journal of experimental biology*, 208(6):979–991, 2005.

Pranav A Bhounsule, Andy Ruina, and Gregg Stiesberg. Discrete-decision continuous-actuation control: balance of an inverted pendulum and pumping a pendulum swing. *Journal of Dynamic Systems, Measurement, and Control*, 137(5):051012, 2015.

Reinhard Blickhan. The spring-mass model for running and hopping. *Journal of biomechanics*, 22(11-12):1217–1227, 1989.

Thomas Buschmann, Sebastian Lohmeier, Mathias Bachmayer, Heinz Ulbrich, and Friedrich Pfeiffer. A collocation method for real-time walking pattern generation. In *Humanoid Robots, 2007 7th IEEE-RAS International Conference on*, pages 1–6. IEEE, 2007.

Katie Byl and Russ Tedrake. Approximate optimal control of the compass gait on rough terrain. In *Robotics and Automation, 2008. ICRA 2008. IEEE International Conference on*, pages 1258–1263. IEEE, 2008.

Germana Cappellini, Yuri P Ivanenko, Richard E Poppele, and Francesco Lacquaniti. Motor patterns in human walking and running. *Journal of neurophysiology*, 95(6):3426–3437, 2006.

Steve Collins, Andy Ruina, Russ Tedrake, and Martijn Wisse. Efficient bipedal robots based on passive-dynamic walkers. *Science*, 307(5712):1082–1085, 2005.

Paolo De Leva. Adjustments to zatsiorsky-seluyanov's segment inertia parameters. *Journal of biomechanics*, 29(9):1223–1230, 1996.

Jiro Doke, J Maxwell Donelan, and Arthur D Kuo. Mechanics and energetics of swinging the human leg. *The Journal of Experimental Biology*, 208(3):439–445, 2005.

Janice J Eng and David A Winter. Kinetic analysis of the lower limbs during walking: what information can be gained from a three-dimensional model? *Journal of biomechanics*, 28(6): 753–758, 1995.

Salman Faraji, Soha Pouya, and Auke Ijspeert. Robust and agile 3d biped walking with steering capability using a footstep predictive approach. In *Robotics Science and Systems (RSS)*, 2014.

Siyuan Feng, X Xinjilefu, Weiwei Huang, and Christopher G Atkeson. 3d walking based on online optimization. In *Humanoid Robots (Humanoids), 2013 13th IEEE-RAS International Conference on*, pages 21–27. IEEE, 2013.

Steven A Gard, Steve C Miff, and Arthur D Kuo. Comparison of kinematic and kinetic methods for computing the vertical motion of the body center of mass during walking. *Human movement science*, 22(6):597–610, 2004.

Mario Gomes and Andy Ruina. Walking model with no energy cost. *Physical Review E*, 83(3):032901, 2011.

Robert D Gregg and Mark W Spong. Bringing the compass-gait bipedal walker to three dimensions. In *Intelligent Robots and Systems, 2009. IROS 2009. IEEE/RSJ International Conference on*, pages 4469–4474. IEEE, 2009.

Robert D Gregg, Adam K Tilton, Sal Candido, Timothy Bretl, and Mark W Spong. Control and planning of 3-d dynamic walking with asymptotically stable gait primitives. *Robotics, IEEE Transactions on*, 28(6):1415–1423, 2012.

Samuel R Hamner, Ajay Seth, Katherine M Steele, and Scott L Delp. A rolling constraint reproduces ground reaction forces and moments in dynamic simulations of walking, running, and crouch gait. *Journal of biomechanics*, 46(10):1772–1776, 2013.

S Javad Hasaneini, CJB Macnab, John EA Bertram, and Henry Leung. The dynamic optimization approach to locomotion dynamics: human-like gaits from a minimally-constrained biped model. *Advanced Robotics*, 27(11):845–859, 2013.

H Hemami and CL Golliday. The inverted pendulum and biped stability. *Mathematical Biosciences*, 34(1):95–110, 1977.

Andrei Herdt, Nicolas Perrin, and P-B Wieber. Walking without thinking about it. In *Intelligent Robots and Systems (IROS), 2010 IEEE/RSJ International Conference on*, pages 190–195. IEEE, 2010.

Fumiya Iida, Yohei Minekawa, Jürgen Rummel, and André Seyfarth. Toward a human-like biped robot with compliant legs. *Robotics and Autonomous Systems*, 57(2):139–144, 2009.

Verne T Inman, Howard D Eberhart, et al. The major determinants in normal and pathological gait. *J Bone Joint Surg Am*, 35(3): 543–558, 1953.

Shuuji Kajita and Kazuo Tani. Study of dynamic biped locomotion on rugged terrain-derivation and application of the linear inverted pendulum mode. In *Robotics and Automation, 1991. Proceedings., 1991 IEEE International Conference on*, pages 1405–1411. IEEE, 1991.

Shuuji Kajita, Fumio Kanehiro, Kenji Kaneko, Kazuhito Yokoi, and Hirohisa Hirukawa. The 3d linear inverted pendulum mode: A simple modeling for a biped walking pattern generation. In *Intelligent Robots and Systems, 2001. Proceedings. 2001 IEEE/RSJ International Conference on*, volume 1, pages 239–246. IEEE, 2001.

Shuuji Kajita, Fumio Kanehiro, Kenji Kaneko, Kiyoshi Fujiwara, Kensuke Harada, Kazuhito Yokoi, and Hirohisa Hirukawa. Biped walking pattern generation by using preview control of zero-moment point. In *Robotics and Automation, 2003. Proceedings. ICRA'03. IEEE International Conference on*, volume 2, pages 1620–1626. IEEE, 2003.

Matthew Kelly and Andy Ruina. Non-linear robust control for inverted-pendulum 2d walking. In *Robotics and Automation (ICRA), 2015 IEEE International Conference on*, pages 4353–4358. IEEE, 2015.

Twan Koolen, Tomas De Boer, John Rebula, Ambarish Goswami, and Jerry Pratt. Capturability-based analysis and control of legged locomotion, part 1: Theory and application to three simple gait models. *The International Journal of Robotics Research*, 31(9):1094–1113, 2012.

Scott Kuindersma, Frank Permenter, and Russ Tedrake. An efficiently solvable quadratic program for stabilizing dynamic locomotion. In *Robotics and Automation (ICRA), 2014 IEEE International Conference on*, pages 2589–2594. IEEE, 2014.

Arthur D Kuo. Stabilization of lateral motion in passive dynamic walking. *The International journal of robotics research*, 18(9): 917–930, 1999.

Arthur D Kuo, J Maxwell Donelan, and Andy Ruina. Energetic consequences of walking like an inverted pendulum: step-to-step transitions. *Exercise and sport sciences reviews*, 33(2): 88–97, 2005.

Ian R Manchester and Jack Umenberger. Real-time planning with primitives for dynamic walking over uneven terrain. In *Robotics and Automation (ICRA), 2014 IEEE International Conference on*, pages 4639–4646. IEEE, 2014.

Christophe Maufroy, H Moritz Maus, and André Seyfarth. Simplified control of upright walking by exploring asymmetric gaits induced by leg damping. In *Robotics and Biomimetics (ROBIO), 2011 IEEE International Conference on*, pages 491–496. IEEE, 2011.

Tad McGeer. Passive dynamic walking. *the international journal of robotics research*, 9(2):62–82, 1990.

Michael B. Monagan, Keith O. Geddes, K. Michael Heal, George Labahn, Stefan M. Vorkoetter, James McCarron, and Paul DeMarco. *Maple 10 Programming Guide*. Maplesoft, Waterloo ON, Canada, 2005.

Katsuhiko Ogata. *Discrete-time control systems*, volume 2. Prentice Hall Englewood Cliffs, NJ, 1995.

Jong H Park and Kyong D Kim. Biped robot walking using gravity-compensated inverted pendulum mode and computed torque control. In *Robotics and Automation, 1998. Proceedings. 1998 IEEE International Conference on*, volume 4, pages 3528–3533. IEEE, 1998.

Juergen Rummel, Yvonne Blum, H Moritz Maus, Christian Rode, and Andre Seyfarth. Stable and robust walking with compliant legs. In *Robotics and Automation (ICRA), 2010 IEEE International Conference on*, pages 5250–5255. IEEE, 2010.

Yoshiaki Sakagami, Ryujin Watanabe, Chiaki Aoyama, Shinichi Matsunaga, Nobuo Higaki, and Kikuo Fujimura. The intelligent asimo: System overview and integration. In *Intelligent Robots and Systems, 2002. IEEE/RSJ International Conference on*, volume 3, pages 2478–2483. IEEE, 2002.

Philippe Sardain and Guy Bessonnet. Forces acting on a biped robot. center of pressure-zero moment point. *Systems, Man and Cybernetics, Part A: Systems and Humans, IEEE Transactions on*, 34(5):630–637, 2004.

Maziar Sharbafi and Andre Seyfarth. Fmch: a new model for human-like postural control in walking. In *Intelligent Robots and Systems, 2015.(IROS 2015). Proceedings. 2015 IEEE/RSJ International Conference on*, volume 1, pages 5742–5747. IEEE, 2015.

Toru Takenaka, Takashi Matsumoto, and Takahide Yoshiike. Real time motion generation and control for biped robot-1 st report: Walking gait pattern generation. In *Intelligent Robots and Systems, 2009. IROS 2009. IEEE/RSJ International Conference on*, pages 1084–1091. IEEE, 2009.

Eric R Westervelt, Jessy W Grizzle, Christine Chevallereau, Jun Ho Choi, and Benjamin Morris. *Feedback control of dynamic bipedal robot locomotion*, volume 28. CRC press, 2007.

JOHN M Workman and BRUCE W Armstrong. Metabolic cost of walking: equation and model. *Journal of Applied Physiology*, 61(4):1369–1374, 1986.

P. Zaytsev, S.J. Hasaneini, and A. Ruina. Two steps is enough: No need to plan far ahead for walking balance. In *Robotics and Automation (ICRA), 2015 IEEE International Conference on*, pages 6295–6300, May 2015. doi: 10.1109/ICRA.2015.7140083.

Appendix A

The parametric matrices C describing 3LP dynamics in single and double support phases are found by Maple. These matrices are sparse and have duplicate elements, since the sagittal and lateral dynamics are similar. Defining auxiliary parameters:

$$\begin{aligned} u &= h_3 + h_1 \\ v &= h_2 - h_1 \\ c_1 &= m_1 u h_1 + m_2 v^2 \\ c_2 &= m_1 u h_1 + 2 m_2 v^2 \\ c_3 &= -m_1 h_1 + m_2 v - m_2 h_1 \\ c_4 &= (-1 + \frac{2t}{t_{ds}}) h_1 + v \end{aligned} \tag{45}$$

the matrices in (8) take the form:

$$\begin{aligned} C_X^{ss} &= \frac{g}{c_1} \begin{bmatrix} (-\frac{c_2}{h_2} + m_2 v) I & \frac{m_1 h_1 (v+u)}{h_2} I & \frac{v c_3}{h_2} I \\ m_2 h_1 I & (m_1 h_1 - m_2 v) I & c_3 I \\ 0 & 0 & 0 \end{bmatrix} \\ C_U^{ss} &= \frac{h_1}{c_1} \begin{bmatrix} \frac{c_2}{h_2^2 m_2} I & -\frac{v}{h_2} I \\ \frac{v}{h_2} I & -I \\ 0 & 0 \end{bmatrix} \\ C_V^{ss} &= \frac{t}{t_{ss}} C_U^{ss} \\ C_W^{ss} &= \frac{h_1}{c_1} \begin{bmatrix} \frac{vu}{h_2} I & -\frac{v}{h_2} I \\ uI & -I \\ 0 & 0 \end{bmatrix} \\ C_d^{ss} &= \frac{g w_P}{c_1} \begin{bmatrix} \frac{c_2}{h_2} J \\ m_2 v J \\ 0 \end{bmatrix} \end{aligned} \tag{46}$$

and the matrices in (21) are found as:

$$\begin{aligned} C_X^{ds} &= \frac{g h_1 m_1}{c_2} \begin{bmatrix} 0 & 0 & 0 \\ (-1 + \frac{t}{t_{ds}}) I & I & -\frac{t}{t_{ds}} I \\ 0 & 0 & 0 \end{bmatrix} \\ &\quad + \frac{g m_2}{c_2} \begin{bmatrix} 0 & 0 & 0 \\ c_4 I & -2vI & c_4 I \\ 0 & 0 & 0 \end{bmatrix} \\ C_U^{ds} &= \frac{h_1}{c_2} \begin{bmatrix} 0 & 0 \\ 0 & I \\ 0 & 0 \end{bmatrix} \\ C_V^{ds} &= (1 - \frac{t}{t_{ds}}) \quad C_U^{ds} \\ C_W^{ds} &= \frac{h_1}{c_2} \begin{bmatrix} 0 & 0 \\ uI & -I \\ 0 & 0 \end{bmatrix} \\ C_d^{ds} &= 0 \end{aligned} \tag{47}$$

where $I \in \mathbb{R}^{2\times 2}$ is identity matrix and $J = [0 \ 1]^T$. The closed form transition matrices in (10) and (21) are then calculated symbolically based on these matrices. Altogether, offline calculations require about $3.7k$ FLOPS in a maple-optimized code which take few microseconds on an average core-i5 computer if implemented in c++. The results are constant matrices in (11) and (11) which can be used online with a much faster speed.